Application performances of two greenhouses with new types of backwall in Yangling, China

Yachen Sun[1,2†*], Haotian Wang[2†], Chenmeng Zhu[3], Hongyi Lyu[2], Xuanhe Zhang[2], Yanfei Cao[2], Jianming Li[2], Zhirong Zou[2], Encai Bao[4*]

(1. *College of Architecture and Urban Planning, Tongji University, Shanghai 200092, China*;
2. *Key Laboratory of Protected Horticultural Engineering in Northwest, Ministry of Agriculture and Rural Affairs, Department of Horticulture, Northwest A&F University, Yangling 712100, Shaanxi, China*;
3. *Office of Academic Affairs*, *Fudan University, Shanghai 200433, China*;
4. *Institute of Agricultural Facilities and Equipment, Jiangsu Academy of Agricultural Science, Key Laboratory of Protected Agriculture Engineering in the Middle and Lower Reaches of Yangtze River, Ministry of Agriculture and Rural Affairs, Nanjing 210014, China*)

Abstract: In order to investigate the application performances of the solar greenhouses with new types of backwalls (greenhouse W_2, and greenhouse W_3) and the ordinary clay brick backwall greenhouse (greenhouse W_1), and provide a theoretical basis for the construction of solar greenhouses in Yangling Demonstration Zone, Shaanxi, China, two greenhouses with different new types of backwall were designed. One of the backwall was built with lightweight aggregate concrete block (greenhouse W_2) and that of the other one was assembled with a row of sand-filled cement pipes (greenhouse W_3). The tested greenhouses were constructed in Yangling Demonstration Zone. Based on the data collected on typical sunny and cloudy days, the indoor temperature, inside wall temperature, and the heat flow of the greenhouses with new types of backwalls were compared with those detected in the ordinary clay brick backwall solar greenhouse, and the tested results were numerically simulated. According to the comparison of the physiological indicators of tomatoes planted in the greenhouses and the construction costs, the greenhouse type with the best practicability was found. The results indicated that: The average air temperature in greenhouses W_1, W_2, and W_3 and outside was 15.1°C, 15.9°C, 17.3°C, and −0.4°C on the night of a sunny day, and the air temperature in W_3 was the highest. The average air temperature in greenhouses W_1, W_2, and W_3 and outside were 9.5°C, 13.3°C, 11.0°C, and −5.5°C on the night of a cloudy day, the air temperature in W_2 was the highest. In the depth of 0-330 mm from the interface of the backwalls, the walls were obviously affected by the solar radiation, and the temperature changed greatly. The wall temperature on the sunny days exhibited an ascending order of W_1, W_2, and W_3, while on the cloudy days was in the ascending order of W_1, W_3, and W_2. The wall of W_3 absorbed the most heat during the daytime and released the most heat at night on a sunny day, while W_2 exhibited the second most heat absorption during the daytime, however, it exhibited the highest heat release at night on a cloudy day, which were almost equaled to its heat absorption. Tomatoes in W_3 grew well and exhibited the highest yield, and this greenhouse had the lowest construction costs. Comprehensively considering the physiological indicators of tomatoes and the corresponding construction costs of greenhouses, W_3 has the best application performance in Yangling Demonstration Zone.

Keywords: application performances, solar greenhouse, backwall, temperature
DOI: 10.25165/j.ijabe.20221503.6097

Citation: Sun Y C, Wang H T, Zhu C M, Lyu H Y, Zhang X H, Cao Y F, et al. Application performances of two greenhouses with new types of backwall in Yangling, China. Int J Agric & Biol Eng, 2022; 15(3): 62–71.

1 Introduction

The application of solar greenhouse in China has developed rapidly since the 1980s. Since the backwall of the greenhouse can absorb solar radiation and store the heat during the daytime and can release them into greenhouse at night, the greenhouse can provide favorable temperature for the crops and thus enable continuous crop production for a whole year. As one of the envelope structures of the solar greenhouse, the walls play not only a load-bearing role, but also have an irreplaceable role in heat preservation and heat storage[1-3]. The previous studies on the thermal environment of greenhouses have provided a basis for further investigation of the thermal environment characteristics of heliostats[4-6]. Research on different wall materials[7-9] and studies on different wall structures[10-12] have shown that the material and structure of the wall are key factors affecting its thermal storage capacity. With the progress of science and technology, the structure of greenhouse walls is continuously optimized[13-15].

Received date: 2020-08-20 **Accepted date:** 2022-01-19
Biographies: Haotian Wang, MS candidate, research interest: facility horticulture engineering, Email: ssyywht@ nwafu.edu.cn; **Chenmeng Zhu**, MS candidate, research interest: organizational management, Email: zhuchenmeng@fudan.edu.cn; **Hongyi Lyu**, MS candidate, research interest: facility horticulture engineering, Email: lvhongyi98@qq.com; **Xuanhe Zhang**, MS candidate, research interest: facility horticulture engineering, Email: 798093267@qq.com; **Yanfei Cao**, PhD, research interest: greenhouse structure optimization, Email: caoyanfei@nwsuaf.edu.cn; **Jianming Li**, PhD, Professor, research interest: facility horticulture, Email: lijianming66@163.com; **Zhirong Zou**, PhD, Professor, research interest: facility horticulture, Email: zouzhirong2005@163.com.

† These authors contribute equally to this work.

***Corresponding author: Yachen Sun**, PhD, research interest: facility horticulture. College of Architecture and Urban Planning, Tongji University, Shanghai 200092, China. Tel: +86-17602144021, Email: sunyachen1993@163.com; **Encai Bao**, PhD, Assistant Research Fellow, research interest: facility horticulture engineering. Jiangsu Academy of Agricultural Science, Nanjing 210014, China. Tel: +86-17768103527, Email: baoencai1990@163.com.

For instance, Zhang et al.[16] reported that using the lead wire fixed gravel as the backwall materials could significantly increase the heat preservation performance of the greenhouse relative to the ordinary brick. Bao et al.[17-20] designed a new composite backwall using porous brick and solidified sand. For further improvement, active heat storage and cycling system were added to the passive heat storage wall. Their results indicated that the greenhouse with inbuilt active heat storage and cycling system composite backwall exhibited obvious higher indoor temperature than those with simple composite backwall or ordinary clay brick backwall. Yang et al.[21] evaluated the thermal insulation and heat storage performance of the brick-polystyrene board composite wall according to a 10 d determination, and stated that the wall with external polystyrene board exhibited better thermal insulation performance than the wall with inbuilt polystyrene board. Agrafiotis et al.[22-24] reported a new type of porous ceramic-foam heat storage material, and a type of solar redox powder was added to this material to improve its heat storage performance. However, although the application of the abovementioned new materials or structures significantly improves the heat preservation performance of the greenhouse, the construction costs of these walls are relatively high, which is adverse to the extensive promotion.

Northwest China is rich in light and heat resources and has a large temperature difference between day and night, which are suitable for the application of solar greenhouses. However, the lack of unified construction standards, the high time or labor consumption, and the poor insulation performance hinder the application of solar greenhouse here[25]. Therefore, the development of low-cost backwalls that is suitable for the local environment is of great significance. Lightweight aggregate concrete block is a type of cost-effective material exhibiting favorable compressive strength and insulation capacity[26-29]. The sand from non-cultivated areas exhibits favorable abilities of heat transfer, heat storage, and thermal conductivity[30]. Using cement pipes filled with sand to form assembled backwalls can save time and labor costs, and the materials are easily obtainable. However, using these materials for the construction of greenhouse backwalls is still not well studied. Hence, in the present study, the thermal environment of solar greenhouses with three different types of backwall (ordinary clay brick backwall (greenhouse W_1), lightweight aggregate concrete block backwall (greenhouse W_2), and the sand-filled cement pipes assembled backwall (greenhouse W_3)) was analyzed and compared, to find out the backwall with the best heat storage performance. The results would provide a scientific basis for the construction of backwalls of the solar greenhouse.

2 Materials and methods

2.1 Structure of tested greenhouses

The studied greenhouse is located in Northwest A&F University, Yangling, Shaanxi, China (108.07°E, 34.27°N), the mean altitude here is 500 m. The length of the tested south-towards greenhouses is 30 m, and the span of them is 10 m. The heights of the backwall and ridge of the studied greenhouse are 3.7 m and 4.4 m, respectively. The greenhouse has a bilayer-film structure, and the crop planted inside is the "Provence" tomato.

For the present study, the mentioned greenhouse was separated into three compartments with 100 mm thick polystyrene boards. In order to ensure uniform experimental conditions, the inner surface of the gables on both sides was also covered with the same polystyrene board. The materials for building the backwalls of the three compartments were ordinary clay brick, lightweight aggregate concrete block, and sand-filled cement pipes, respectively. Clay brick had a length of 240 mm, a width of 50 mm, and a thickness of 210 mm. The lightweight aggregate concrete block had a length of 600 mm, a width of 200 mm, and a thickness of 235 mm. The cement pipes had a diameter of 500 mm, a height of 3 m, and a pipe wall thickness of 50 mm. The pipes were filled with 0.377 m^2 of building sand, and 20 pipes were assembled as a backwall, the top of them was connected with a 0.7 m height clay brick wall. The specifications of the three compartments and the picture of the backwalls are shown in Figures 1 and 2.

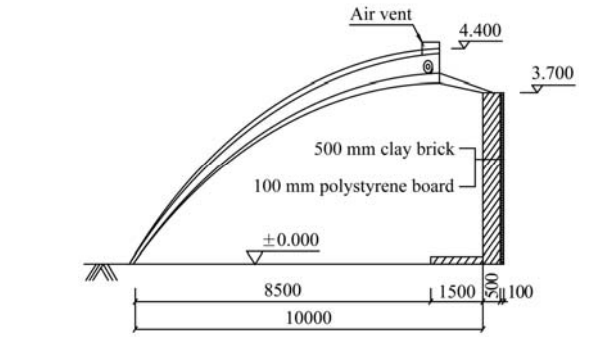

a. Solar greenhouse W_1

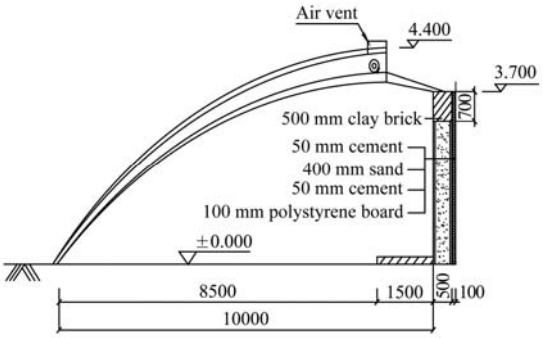

b. Solar greenhouse W_2

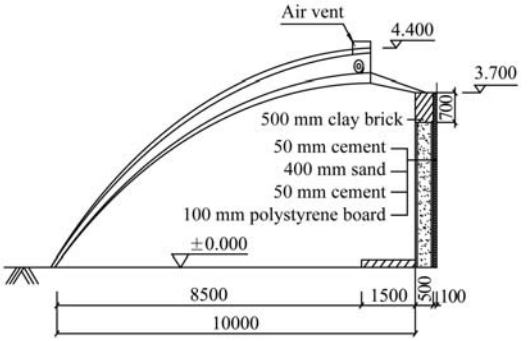

c. Solar greenhouse W_3

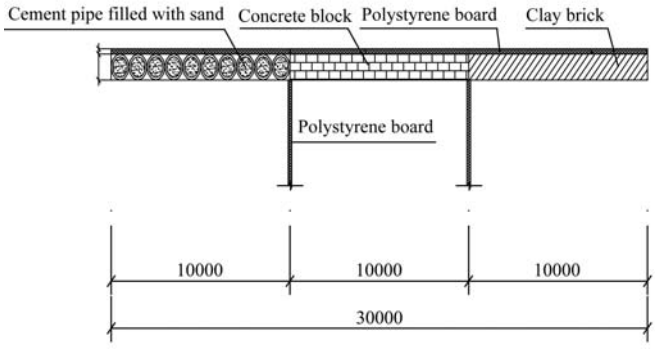

d. Floor plan of the backwalls

Figure 1 Structure of the tested greenhouses (mm)

a. Ordinary clay brick backwall

b. Lightweight aggregate concrete block backwall

c. Sand-filled cement pipes assembled backwall

Figure 2 The backwalls tested in this study

2.2 Data collection

The measuring points were set as shown in Figure 3, Points 1 and 2 were set for detecting the indoor air temperature and humidity, Point 3 was set for detecting the outside air temperature, humidity, and illumination intensity. Points 4 and 6 were set for detecting the indoor soil temperature and illumination intensity, respectively. Point 5 was set for detecting the outside soil temperature, which was set at a depth of 150 mm in the soil. Points 7 and 11 were set for detecting the heat flux density on the surface of the backwall, while Points 8-10 and 12-14 were set for detecting the inside temperature of the backwall, which were set in the depths of 160 mm, 330 mm, and 500 mm in the backwall, respectively.

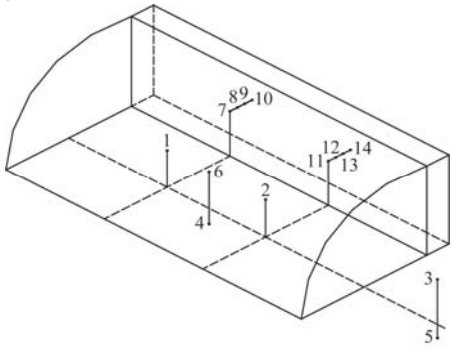

Note: Points 1 and 2 were set for detecting the indoor air temperature and humidity; Point 3 was set for detecting the outside air temperature, humidity, and illumination intensity; Points 4 and 6 were set for detecting the indoor soil temperature and illumination intensity, respectively; Point 5 was set for detecting the outside soil temperature, which was set at a depth of 150 mm in the soil; Points 7 and 11 were set for detecting the heat flux density on the surface of the backwall, while Points 8-10 and 12-14 were set for detecting the inside temperature of the backwall, which were set in the depths of 160 mm, 330 mm, and 500 mm in the backwall, respectively.

Figure 3 Distribution of environmental measuring points

The data were collected from November 2017 to March 2018. A typical sunny day (January 19, 2018) and a typical cloudy day (January 7, 2018) were chosen for comparison. During the experiment, the insulation quilt on the front roof was uncovered at 9:00 a.m. and covered at 17:30 on sunny or cloudy days, while it was maintained covered on snowy days.

The indoor and outside environmental data, including the air temperature and humidity, and the illumination intensity, were collected by a HOBO portable small automatic meteorological station (Onset Co. Ltd., USA) every 30 min. The measurement range of temperature of the meteorological station was −40°C-75°C, the resolution was 0.4°C, and the accuracy was ±0.7°C. The wall temperature, soil temperature, and the heat flux at the inner surface of the backwall were collected using an Agilent 34970A data acquisition (Agilent Co. Ltd., USA) every 30 min.

3 Results

3.1 Inside and outside illumination intensity of the greenhouse

Indoor illumination intensity indicates the light conditions of the greenhouse, while it also controls the heat storage and release of the backwall. Hence, the analysis of the illumination intensity of the three compartments was the premise of this study[21,31-34].

On both sunny and cloudy days, the changes in the indoor illumination intensity of the three compartments exhibited a similar tendency (Figure 4). The average illumination intensity of the compartments W_1, W_2, and W_3 on a sunny day (9:00-17:30) was 53 984 lx, 53 706 lx, and 53 515 lx, respectively, while the outside average illumination intensity was 77 089 lx. The average indoor illumination intensity of the compartments W_1, W_2, and W_3 on a cloudy day (9:00-17:30) was 7786 lx, 7446 lx, and 7730 lx respectively, while the outside average illumination intensity was 13 771 lx. There was no significant difference in the indoor illumination intensity of the three compartments on both sunny days and cloudy days, indicating that illumination intensity was not the main factor affecting the changes in the indoor temperature of the compartments.

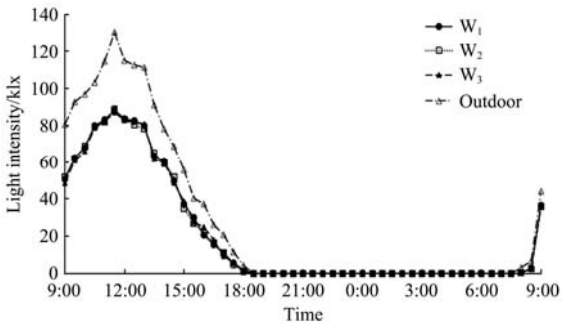

a. Sunny day (January 19, 2018)

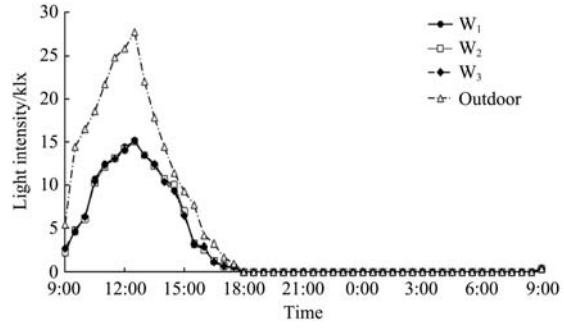

b. Cloudy day (January 7, 2018)

Note: Greenhouse W_1: Ordinary clay brick backwall; Greenhouse W_2: Lightweight aggregate concrete block backwall; Greenhouse W_3: The sand-filled cement pipes assembled backwall. The same as below.

Figure 4 Variation of the indoor and outside illumination intensity of the three compartments

3.2 Indoor and outside air temperature of the greenhouse

As shown in Figure 5a, the diurnal variation of the air temperature in compartments W_1, W_2, and W_3 and outside on

typical sunny days (from 9:00, Jan. 19 to 9:00, Jan. 20, 2018) exhibited a similar tendency. The lowest outside temperature was observed at 5:00, while the lowest indoor temperatures of W_1, W_2, and W_3 were observed at 8:00, because there was no heat entered before the insulation quilt was uncovered, leading to the continuous decrease in the indoor temperature. The average air temperatures in W_1, W_2, and W_3 and outside at night on sunny days (17:30-9:00) were 15.1°C, 15.9°C, 17.3°C, and −0.4°C, respectively, while the lowest air temperatures in W_1, W_2, and W_3 and outside were 12.4°C, 14.2°C, 14.4°C, and −2.8°C. Both the average and lowest indoor temperatures in W_3 were significantly higher than those in W_2 and W_1, that was, W_3 exhibited better heat preservation performance at night on typical sunny days.

As shown in Figure 5b, the diurnal variation of the air temperature in W_1, W_2, and W_3 and outside on a typical cloudy day (from 9:00, Jan. 7, to 9:00, Jan. 7, 2018) also exhibited a similar tendency, however, the temperatures were generally lower than those detected on the sunny day. All the lowest temperatures in the three compartments and outside were observed at 8:00. The average temperatures in W_1, W_2, and W_3 and outside at night on cloudy days (17:30-9:00) were 11.5°C, 14.8°C, 13.0°C, and −3.0°C, respectively, while the lowest temperatures in W_1, W_2, and W_3 and outside were 7.5°C, 11.3°C, 9.1°C, and −10.3°C. Both the average or lowest indoor temperatures of W_2 were significantly higher than those of W_3 and W_1, that was, W_2 exhibited better heat preservation performance at night on typical cloudy days.

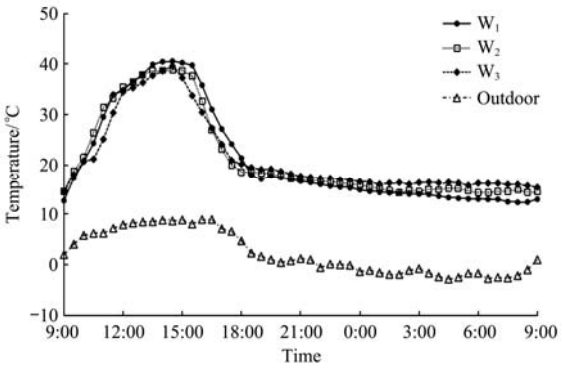

a. The sunny day (January 19, 2018)

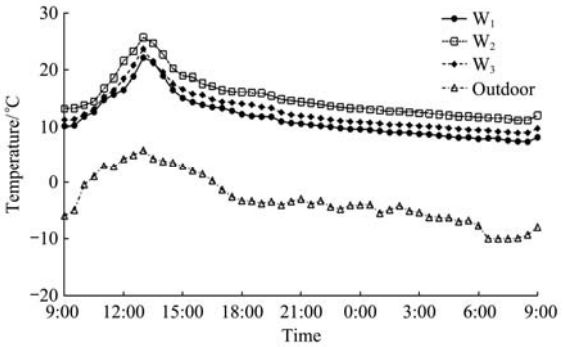

b. The cloudy day (January 7, 2018)

Figure 5 Variation of the indoor and outside air temperature of the three compartments

3.3 Inside temperature at different depths in the backwalls

The backwall plays an important role in maintaining the heat balance of the solar greenhouse. Its heat storage capacity is critical to the thermal performance of the greenhouse. The temperature change and distribution in the backwall reflect the heat exchange process between the backwall and the indoor air. They also reflect the ability of the heat contribution of the backwall, which greatly affects the indoor temperature of the greenhouse at night[25]. In the present study, the inside temperatures of the backwalls in the depths of 160 mm, 330 mm, and 500 mm from their inner surface were selected for comparative analysis.

Figure 6 exhibited the daily variation of the temperature at different depths of the backwalls during a typical sunny day. The inside temperature of the walls exhibited significant decreases as the depth increases. The maximum daily temperature differences of the walls of W_1, W_2, and W_3 were 12.5°C, 13.7°C, and 11.1°C in the depth of 160 mm, while those differences were 3.1°C, 2.3°C, and 2.2°C in the depth of 330 mm, and 2.1°C, 1.4°C, and 0.9°C in the depth of 500 mm indicating that the temperature change of the wall became less obvious as the increases in the depth. The average daily temperatures of the walls of W_1, W_2, and W_3 were 17.0°C, 18.9°C, and 19.4°C in the depth of 160 mm, while the average temperatures were 13.4°C, 14.0°C, and 14.8°C in the depth of 330 mm, and 8.8°C, 11.1°C, and 11.9°C in the depth of 500 mm. The inside temperature of backwall exhibited an ascending order of W_1, W_2, and W_3, indicating that the backwall of W_3 exhibited favorable heat storage and insulation capabilities under typical sunny weather conditions. As for the diurnal variation of the inside temperature of backwalls, the temperature in the depth of 160 mm decreased firstly, and it increased after the insulation quilt was uncovered, and then decreased again after the quilt was covered again at night. This pattern was similar to the diurnal variation of the inside air temperature, indicating that the temperature change in the depth of 0-160 mm of the backwall was significantly affected by the change in indoor air temperature. In the depth of 330 mm, the diurnal variation of the inside temperature of backwalls exhibited a similar pattern to that in the depth of 160 mm, however, the range of variation was obviously smaller. In the depth of 500 mm, an obvious increase and decrease of temperature only occurred during 10:30-16:30.

During a typical cloudy day, the inside temperature of the backwalls also exhibited a decreasing tendency with the increase in depth (Figure 7). However, the range of the decreases was less obvious relative to that on the sunny day, which was attributed to the less obvious changes in the indoor air temperature caused by the weaker solar radiation. The maximum daily temperature differences of the walls of W_1, W_2, and W_3 were 5.7°C, 6.3°C, and 6.3°C in the depth of 160 mm, while those differences were 3.8°C, 5.5°C, and 4.8°C in the depth of 330 mm, and 1.0°C, 0.7°C, and 1.1°C in the depth of 500 mm. These indicated that the temperature change of the wall also became less obvious as the increases in the depth like on the sunny days. The average daily temperatures of W_1, W_2, W_3 were 12.5°C, 14.4°C, and 13.1°C in the depth of 160 mm, while the average temperatures were 10.5°C, 12.1°C, and 11.5°C in the depth of 330 mm, and 7.0°C, 8.4°C, and 7.5°C in the depth of 500 mm, which all were significantly lower than those detected on the sunny days. The inside temperature of backwall exhibited an ascending order of W_1, W_3, W_2, indicating that the backwall of W_2 exhibited favorable heat storage and insulation capabilities under the typical cloudy weather condition. The diurnal variation of the inside temperature of backwalls on the cloudy days exhibited a different tendency from that on the sunny days. The inside temperature in the depth of 160 mm of walls decreased firstly, and it exhibited an increasing tendency after the insulation quilt was uncovered until 1 h after the quilt was covered, and then decreased. The highest inside temperature of backwalls occurred later on the cloudy days than those on the

sunny days, intuitively, the curves of temperature variation moved to the right. These might be caused by the lower temperature of the air and walls under cloudy conditions, which led to slower temperature changes. In the depth of 330 mm, the changes in the inside temperature exhibited a similar tendency as those in the depth of 160 mm, however, the decreases in temperature were less obvious (only 1°C-2°C). In the depth of 500 mm, the inside temperature of backwalls exhibited no significant changes.

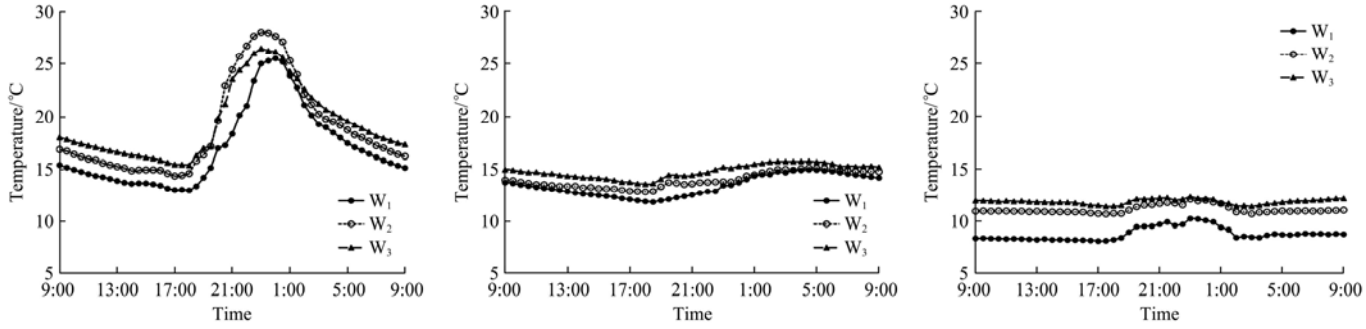

a. 160 mm b. 330 mm c. 500 mm

Figure 6 Daily variation of the temperature in different depths of the backwalls on sunny days

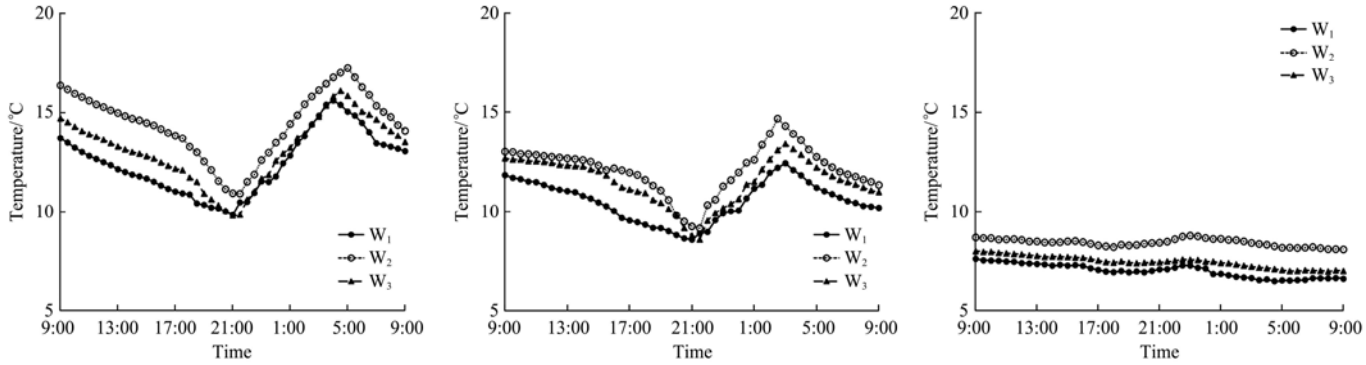

a. 160 mm b. 330 mm c. 500 mm

Figure 7 Daily variation of the temperature in different depths of the backwalls on cloudy days

3.4 Heat flux density changes and comparisons of heat storage and release

3.4.1 Heat flux density changes of the backwalls in different weather conditions

Figure 8 exhibited the heat flux density changes in the tested backwalls on typical sunny or cloudy days, in which the positive values indicated the heat transfer from indoor air to the walls, and negative values exhibited opposite transfer directions. The backwalls absorbed solar radiation to store heat during the daytime and released it into the greenhouse at night.

On the sunny days, before the insulation quilt was uncovered (17:30-9:00 of the next day), the average heat flux densities of the backwalls of W_1, W_2, and W_3 were 9.05 W/m^2, 9.44 W/m^2, and 11.51 W/m^2, respectively. The walls released heat into the greenhouse, the differences in heat flux among the three compartments were negligible, and the change range of heat flux was relatively stable. When the quilt was uncovered (9:00-17:30), the walls received solar radiation and absorbed heat rapidly, thus the heat flux density kept increasing. The heat flux density of the three greenhouses reached their daily maximum values of 181.0 W/m^2, 191.1 W/m^2, and 202.4 W/m^2, respectively, at 12:00-13:30, and then the heat flux of the walls exhibited continuous decreases. When the quilt was covered (about 17:30), the walls began to radiate heat to the greenhouse, and the heat flux of W_3 was significantly higher than those of W_2 and W_1. The heat release gradually increased, and became stabilized after 21:00. The average nighttime value and the maximum daily heat flux density of W_3 were the highest, indicating that W_3 exhibited favorable heat storage and release capacity on a typical sunny day.

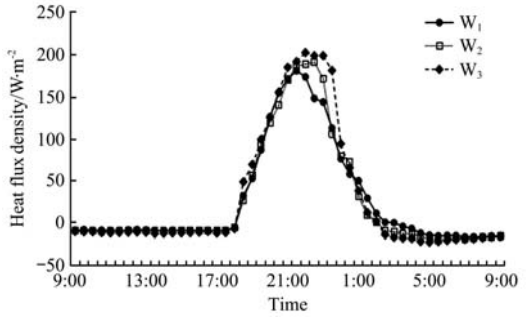

a. The sunny day (January 19, 2018)

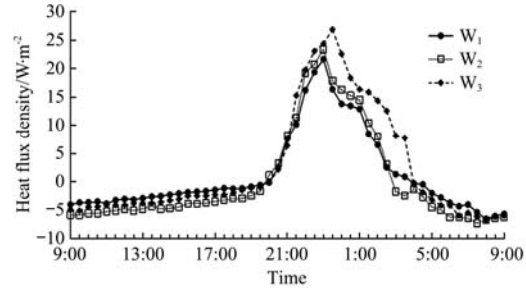

b. The cloudy day (January 7, 2018)

Figure 8 Heat flux density changes of the tested backwalls

On a cloudy day, the solar radiation was weak, thus less heat could be received and stored in each compartment, and the heat flux density of them was also smaller than that on sunny days. In addition, the time for heat to flow into the walls from the air was significantly delayed to about 11:30, the reason was that the weak radiation led to slow increases in indoor air temperature, thus the heat still flowed into the air from the walls. Subsequently, as the

indoor air temperature increased, the heat flux of the three compartments also increased. W_1 and W_2 reached their daily maximum heat flux values of 21.67 W/m^2 and 23.40 W/m^2 at 14:00, respectively, while W_3 reached a daily maximum value of 26.91 W/m^2 at 14:30. The average heat flux density of the walls in the endothermic state during the day was 10.28 W/m^2, 12.38 W/m^2, and 15.63 W/m^2 respectively, which were similar to the pattern on the sunny days (W_3>W_2>W_1). After the quilt was covered (17:30), the indoor air temperature exhibited continuous decreases, and the walls began to release heat into the air at about 19:00. In the heat release state at night, the backwall of W_2 exhibited higher heat flux density (4.44 W/m^2) than those of W_3 and W_1 (2.70 W/m^2 and 3.49 W/m^2, respectively).

3.4.2 Heat storage and release efficiency of the backwalls in different weather conditions

The heat storage and release were important parameters for evaluating the thermal performance of backwall, indicating their abilities in heat absorption and thermal insulation. Figure 9 exhibited the heat change per unit area of the inner surface of the backwalls under two typical weather conditions. On sunny days, the backwalls absorbed more heat from the intense radiation, the heat absorption of the backwalls of W_1, W_2, and W_3 were 2.87 MJ/m^2, 2.94 MJ/m^2, and 3.32 MJ/m^2 in the daytime, while the heat release of them after the quilt was covered at night were 0.57 MJ/m^2, 0.68 MJ/m^2, and 0.82 MJ/m^2. Obviously, the heat absorbed by the walls was much higher than that was released, indicating that part of the heat was lost to the outside, remained heat was stored in the walls. This heat would be released when there were continuous cloudy days or extreme weather to maintain the indoor temperature of the greenhouse, which was the heat storage mechanism of the greenhouse. Both the heat absorption and release of the backwalls exhibited the same descending order of W_3, W_2, W_1.

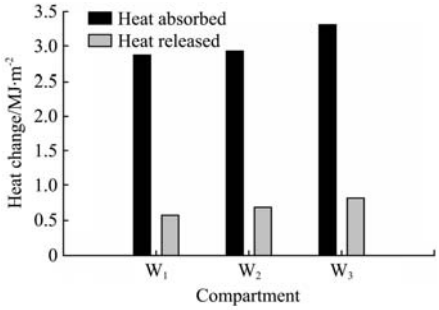

a. The sunny day (January 19, 2018)

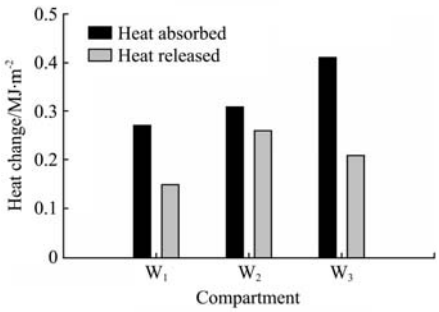

b. The cloudy day (January 7, 2018)

Figure 9 Heat storage and release in back wall of the three compartments

Because of the weak solar radiation, both the heat storage and release of the backwalls were relatively lower on cloudy days. The heat absorbed by the backwalls of W_1, W_2, and W_3 were 0.27 MJ/m^2, 0.31 MJ/m^2, and 0.41 MJ/m^2, respectively, while the heat released from the walls were 0.15 MJ/m^2, 0.26 MJ/m^2, and 0.21 MJ/m^2 after the quilt was covered. The differences between heat storage and release were 0.12 MJ/m^2, 0.05 MJ/m^2, and 0.20 MJ/m^2. These indicated that the heat absorption of the backwall of W_2 was less than that of the backwall of W_3, however, it exhibited the highest heat release at night, which even almost equaled its heat absorption in the daytime. This phenomenon might be caused by the better heat storage of the backwall of W_2, only a little of the heat in the backwall would be released outside, and most of the stored heat on sunny days could be used for mitigating the low temperature inside the greenhouse.

3.5 Numerical model of the temperature of indoor air and wall

Computational fluid dynamics (CFD) uses numerical calculation methods to solve mathematical equations reflecting the flow of fluid with computers, and derive the laws of fluid motion. ANSYS FLUENT, CFX, STAR CCM+, etc. were the most widely used CFD software, in which, FLUENT contains more physical models, more accurate calculation methods, and processing functions than other software, and can be used to simulate more complex flows. It can be used to simulate the steady and transient flow of air in the greenhouse, the convection heat transfer between the air and the backwall, and the solar radiation model. In the present study, ANASYS FLUENT R19 was used to conduct CFD numerical simulation of the indoor air temperature and the heat storage of the backwall of the greenhouses[35]. The grid partitioning of the model was conducted by ICEM CFD and FLUENT MESHING software before CFD numerical simulation.

3.5.1 Simplification of the physical model of the backwall

After receiving solar radiation, the temperature of the backwall and its heat exchange with the surrounding air gradually increased. The closer to the surface of backwall, the greater the heat exchange intensity between the air and the backwall. In this condition, the physical process of convection heat transfer would be more complicated and unstable, which makes the numerical simulation calculation process more difficult. Hence, it was necessary to build a model to calculate the air temperature field in the greenhouse and the heat distribution of the backwall.

In the present study, the tested greenhouses and their backwalls were modeled using NX10.0 with a ratio of 1:1. The north center of each backwall was set as the origin of the modeling coordinates, the length direction of the wall was set as the *Y* direction, the thickness direction was set as the *X* direction, and the height direction was set as the *Z* direction. The model simplifications of W_1, W_2, and W_3 are shown in Figure 10, in which, seams among the bricks or concrete blocks were simplified as smooth surfaces. In addition, the polystyrene board layers on the north side of backwalls were removed in the models, and the effects of air vents were also ignored.

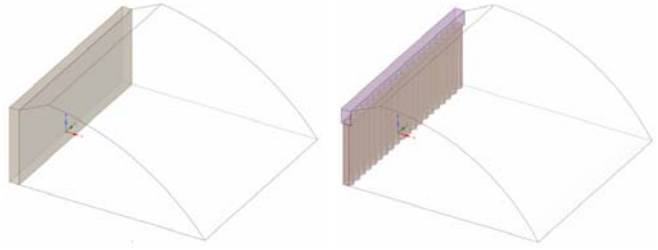

a. W_1 and W_2 b. W_3

Figure 10 Physical models of the backwall of the three compartments

3.5.2 Grid partitioning and the grid independence test

The grid is one of the important factors that affect the accuracy

of computing. Generally, fine grids are more accurate than coarse grids, but the increase in the number of grids will lead to a sharp increase in the costs of computing. Therefore, there is a certain trade-off between the time-consuming and accuracy of the calculation. The number of grids should be within the acceptable range for the calculation accuracy, while the cost of the calculation, such as time, must be within the acceptable range as well.

In order to minimize the number of grids and ensure calculation accuracy, the fluid domain in compartments W_1 and W_2 and the solid domain was partitioned using hexahedral grids, and the nodes of the fluid-solid conjugate plane remained consistent. For W_3, there was more irregular geometry due to the presence of cement pipes and the filled sand, thus the model was partitioned using polyhedral grids, and the nodes of the fluid-solid coupling surface remained consistent.

In order to verify the independence of the calculation results and the number of grids, the models for W_1 and W_3 were selected, and the independence test was performed based on the temperature data detected on the measuring points, which were located in the center of backwalls (Table 1 and Figure 10). The temperature data were collected after 21:00 on January 19. For W_1, the temperature change tended to be stable and was close to the temperature of the measuring point when the grid number reached 224 690. For W_3, this grid number was 415 997. Comprehensively considering the calculation accuracy and time-consuming, scheme C was chosen for the following numerical calculation for W_1 and W_3, and W_2 shared the same grid number as W_1. The grid of the overall computing domain of the greenhouse is shown in Figure 11.

Table 1 Grid numbers of meshes corresponding to measuring point temperature

Compartments	Schemes	Grid numbers	Temperature of the measuring points/°C
W_1 and W_2	A	134 814	10.56
	B	179 752	11.32
	C	224 690	11.78
	D	269 628	11.81
W_3	A	249 598	12.60
	B	332 799	13.13
	C	415 997	13.52
	D	499 196	13.62

Note: A, B, C, and D represent the number of Grid.

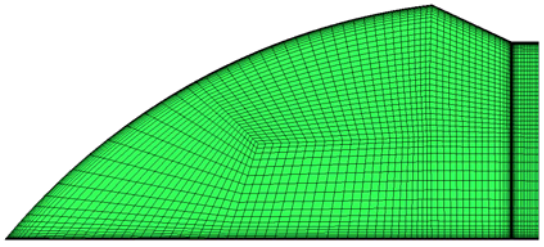

a. W_1 and W_2

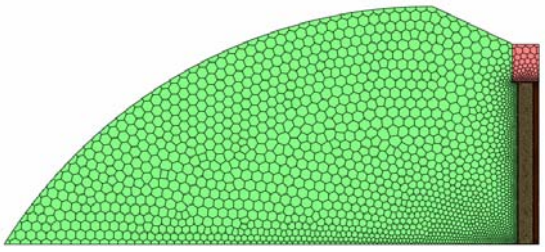

b. W_3

Figure 11 Grid partition method of the overall computing domain of the three compartments

3.5.3 Assumptions for calculation and mathematical model

Three main assumptions were made for the analyses of heat balance: 1) the condensation of water vapor in the air was ignored; 2) the thermal contact resistances between backwalls and soil or greenhouse were ignored; 3) The temperature of the soil surface and the envelope which participated the heat transfer was uniform.

Boussinesq assumption: In the numerical calculation of the natural convection heat transfer in a closed cavity, in order to facilitate the handling of air flow caused by temperature differences, the Boussinesq assumption is often used. That is, the viscous dissipation in the fluid is ignored; for the density, only the terms related to volumetric force in the momentum equation were considered, and in other terms, the density was seen as a constant value, and the method of the FLUENT processing is to add source terms to the momentum equation as follows:

$$S=(\rho-\rho_0)g \tag{1}$$

in which,

$$\rho\approx\rho_0(1-\beta(T-T_0)) \tag{2}$$

$$S=-\rho_0\beta(T-T_0)g \tag{3}$$

where, S is the heat source term in the fluid, J; ρ is the density of the object, kg/m^3; T is the measured temperature, °C; g is the acceleration of gravity, m/s^2, which is 9.8 m/s^2; ρ_0 is the gas density constant, kg/m^3, which is 1.29 kg/m^3; β is the thermal expansion coefficient; T_0 is the reference temperature, °C, which is 20°C; the negative sign indicates that the temperature difference causes the "natural flow" of the hot fluid in the opposite direction of gravity.

The selection of radiation model: Based on the data of latitude and longitude coordinates, the radiation intensity, and solar radiation angle at different times could be calculated according to the solar radiation model in FLUENT, and the influence of the external solar radiation sources could be added into the energy equation. According to the DO irradiation method, the radiative heat flux was loaded to the boundary of the translucent wall, and the solution of the radiative heat source in the DO radiation transport equation was obtained.

$$\nabla\cdot((\vec{r},\vec{s})\vec{s})+(a+\sigma_s)I(\vec{r},\vec{s})=an^2\frac{\sigma T^4}{\pi}+\frac{\sigma_s}{4\pi}\int_0^{4\pi}I(\vec{r},\vec{s})\Phi(\vec{s},\vec{s'})\mathrm{d}\Omega' \tag{4}$$

where, ∇ is the vector partial derivatives; $\vec{r}$ and $\vec{s}$ are the position and direction vectors, respectively; $\vec{s'}$ is the scattering direction vector; a is the absorption coefficient; σ_s is the scattering coefficient; I is the radiation intensity; n is the refractive coefficient; σ is Stephen Boltzmann constant, which is 5.6697 W/m^2·k^4; T is the temperature of Yangling Demonstration Zone, °C, which is 20°C; Φ is the phase function; Ω' is the solid angle of the space.

The selection of turbulence model: Turbulence is a highly complex three-dimensional unsteady motion. The physical parameters in turbulence, such as velocity and pressure, change with time and space without obvious regularity. In the present study, the Reynolds time-average method was used to simulate the air flow, and the RNG K-ε turbulence model within the k-ε turbulence model, which has a good correlation between the added value and the time average was selected.

The boundary conditions: The boundary types of the model were defined in FLUENT, soil surface was defined as the temperature that changed with time, the east and west walls of the greenhouse were defined as symmetry planes, the Po film was defined as the translucent wall, the inner surface of the backwall was defined as the boundary of convective heat transfer, while the contact area of the backwalls and greenhouses was defined as a coupling heat transfer wall.

3.5.4 Results of simulation

When the insulation quilt was covered, the status of soil temperature, backwall temperature, and indoor air temperature was complicated. Hence, the distribution of the air temperature field and backwall temperature field in the three compartments were analyzed based on the data collected at 18:00 on a typical sunny day. At this time, there was obvious stratification of the indoor air temperature field (Figure 12), and the high-temperature region appeared in the middle and upper parts of the greenhouse. Because the temperature of the greenhouse surface was higher than that of the outside, the temperature gradually decreased outwards along the thickness direction of the backwall, and in 0-330 mm inside part of the backwalls, the temperature decreased more rapidly.

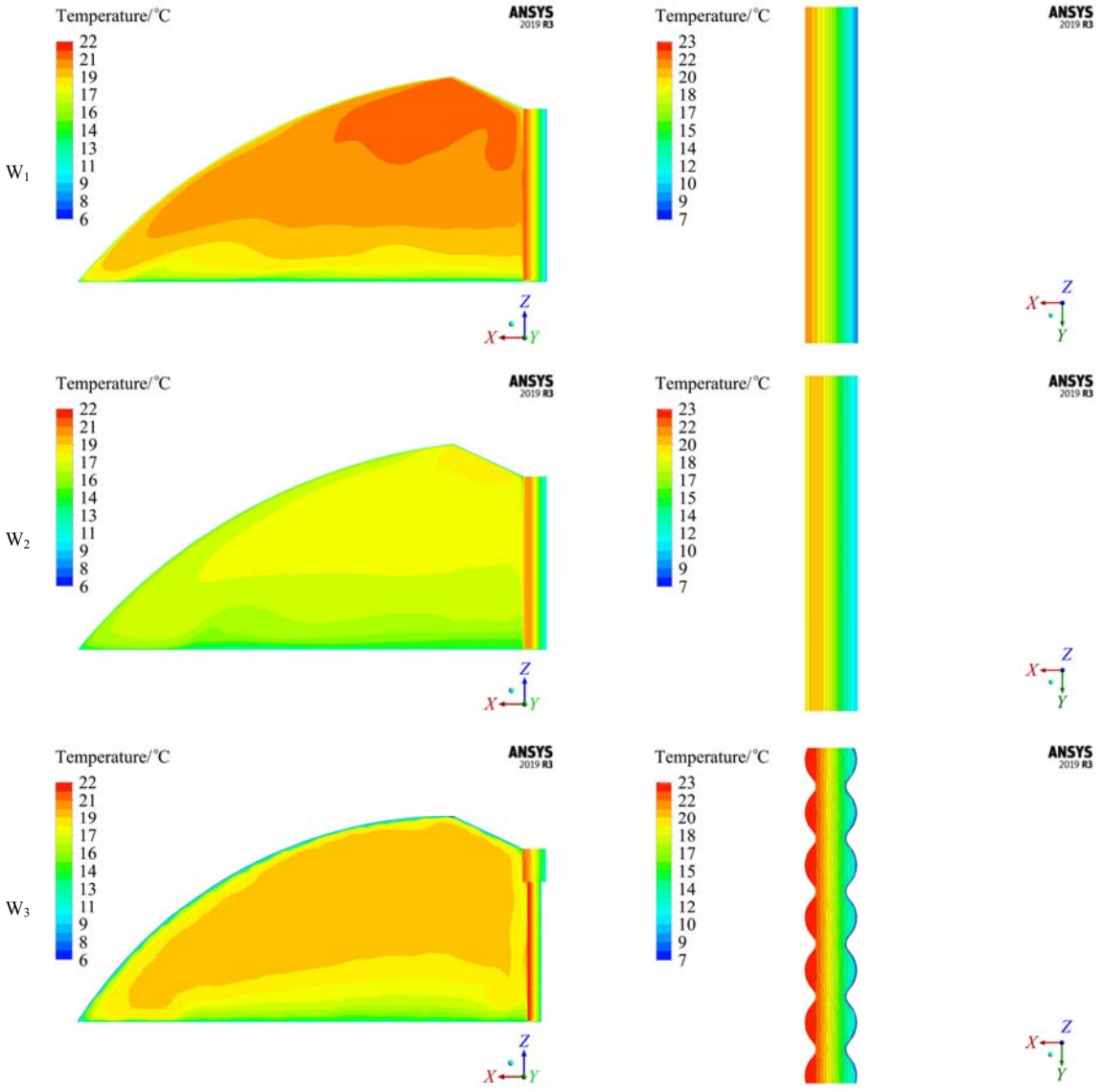

a. Compartments (side view) b. Backwalls (top view)

Figure 12 Thermal environment simulation of the three compartments

For the indoor air temperature field, because the insulation quilt was just covered at this time, the indoor temperature in W_1 was still the highest, just as it performed in the daytime. However, for the inside temperature of backwall, the temperature of W_3 was significantly higher than those of W_2 and W_1, indicating that the greenhouse was now in a transition period of temperature, that was, the backwall temperature gradually dominated the air temperature. With the loss of heat in the greenhouse, the role of the wall gradually emerged. For the three compartments, the backwall of W_3 exhibited the highest temperature and heat storage, thus it released the most heat to the indoor air, leading to much higher indoor temperatures than the other two compartments. These results of the simulation were consistent with the mentioned data of the backwall temperature.

Comparing the temperature change of the measuring points in the simulated or actual backwalls, the maximum absolute error of the simulated and tested values was 1.6°C, the maximum relative error was 11.4%, and the average relative error was 5.3%. These indicated that the simulated and tested values exhibited favorable goodness of fit, and thus the model could be used for the simulation and analyses of the heat transfer of the backwalls of the solar greenhouse.

3.6 Economic benefits of the solar greenhouse

3.6.1 The physiological indicators of tomato

The plant height, stem diameter, single fruit weight, and the yield per plant of tomato after 82 d since plantation were analyzed (Table 2). In the fruiting period, both the plant height and stem diameter of the tomatoes in compartment W_3 were significantly

higher than those in compartments W_2 and W_1. The single fruit weight of tomatoes in W_3 was 16.28 g and 30.18 g more than those in W_2 and W_1, respectively. The yield per plant of tomato in W_3 was 0.14 kg and 0.25 kg more than those in W_2 and W_1, with increases of 13.3% and 22.1%, respectively.

Table 2 Physiological indicators of tomato

Compartments	Height/cm	Stem diameter/mm	Single fruit weight/g	Yield per plant/kg
W_1	78.9^c	7.54^b	154.23^c	1.13^c
W_2	92.4^b	8.53^b	168.13^b	1.27^b
W_3	113.1^a	9.75^a	184.41^a	1.38^a

3.6.2 Construction cost of the greenhouse

The construction cost of the greenhouse is also an important part that determines the economic benefits. The excessive cost is not conducive to the promotion and application of the greenhouse. Compared with W_1, the construction costs of W_2 increased by 15.6 RMB Yuan/m^2, while that of W_3 reduced by 30.9 RMB Yuan/m^2. The lowest cost of W_3 was attributed to the low cost of the backwall materials used. In addition, as the backwall of W_3 was an assembled wall, the labor cost was also lower. On the contrary, because of the expensive wall materials used, W_2 exhibited higher costs than W_1.

Table 3 Construction costs of different tested greenhouse

Items	W_1/ RMB Yuan·m^{-2}	W_2/ RMB Yuan·m^{-2}	W_3/ RMB Yuan·m^{-2}
Steel skeleton	67.2	67.2	67.2
Foundation	39.3	39.3	39.3
Walls	147.8	162.5	121.2
Film, insulation quilt, and automatic control system	53.4	53.4	53.4
Others	14.2	15.3	10.1
Total	321.9	337.5	291.0

3.6.3 Physical properties of different materials

In theory, any substance can be used as a heat storage material. However, in addition to thermal properties such as thermal conductivity and specific heat capacity, its practicality, stability, weather ability and economy limit its applicability. Therefore, we need to continuously develop new wall materials, which are convenient to obtain and adapt to local conditions. Lightweight aggregate concrete blocks have low material cost, high compressive strength, and good heat storage capacity. Sandy soil in non-cultivated areas has good heat transfer, heat storage, and thermal conductivity characteristics. Fill them into hollow cement pipes and arrange them closely. After forming the cement pipe sand column assembled back wall, the advantage is that it is convenient to obtain materials, saves labor and time, and conforms to the law of sustainable development.

The physical properties of the material are shown in Table 4.

Table 4 Physical properties of different materials

Materials	Density /kg m^{-3}	Specific heat capacity /J·kg^{-1}·$°C^{-1}$	Thermal conductivity /W·m^{-1}·$°C^{-1}$
Air	1.29	1013	0.027
Clay bricks W_1	2400	920	0.810
Lightweight aggregate concrete blocks W_2	1700	1030	0.670
Cement W_3	1800	1050	0.930
Sand W_3	2100	1010	0.620
Soil	1400	837	1.520
Po film	900	2550	0.290

4 Conclusions and discussion

Based on the detection of various environmental indicators of three solar greenhouse compartments in different climate conditions, their application performance was comprehensively evaluated. The main conclusions were as follows:

1) The average air temperature in compartments W_1, W_2, W_3, and outside was 15.1°C, 15.9°C, 17.3°C, and −0.4°C on the night of a sunny day, the air temperature in W_3 was the highest. The average air temperature in compartments W_1, W_2, and W_3 and outside was 9.5°C, 13.3°C, 11.0°C, and −5.5°C on the night of a cloudy day, the air temperature in W_2 was the highest.

2) In the depth of 0-330 mm from the inner surface, the temperature of the backwalls was obviously affected by the solar radiation and changed greatly. On a sunny day, the wall temperature of W_3 was slightly higher than that of W_2, while it was significantly higher than that of W_1, indicating that W_3 exhibited favorable heat storage and insulation capabilities. On a cloudy day, the inside temperature of the backwall in any depth was lower than that on a sunny day. The wall temperature of W_2 was higher than those of W_3 and W_1, and the temperature of W_1 was lower than W_3, indicating that W_2 exhibited favorable heat storage and insulation capabilities.

3) During the daytime of sunny days, the heat storage of the backwalls of W_1, W_2, and W_3 were significantly higher than their heat release, and the heat was stored in the walls. The wall of W_3 absorbed more heat during the daytime, and it released more heat at night. On the cloudy day, the differences between the heat storage and release of the backwalls of W_1, W_2, and W_3 were 0.12 MJ/m^2, 0.05 MJ/m^2, and 0.20 MJ/m^2, although the heat absorption was lower than that of the wall of W_3, the wall of W_2 exhibited the highest heat release at night, which even equaled to the heat absorption during the daytime.

4) Tomatoes in W_3 grew well and exhibited the highest yield, and this compartment exhibited the lowest construction costs.

In conclusion, compartment W_3 exhibited the best thermal performance on the sunny day, while W_2 performed the best on the cloudy day. During the period of data collection, there were 72% sunny days, 18% cloudy days, and 10% snowy days, the proportion of sunny days was the highest. Comprehensively considering the physiological indicators of tomatoes and the corresponding construction costs of greenhouses, type W_3 has the best application performance in Yangling Demonstration Zone, China.

Acknowledgements

This research was financially supported by the Shaanxi Provincial Key Research and Development Program (Grant No. 2019TSLNY01-03); the National Natural Science Foundation of China (Grant No. 31901420); the Young Scientist Promotion Project of Jiangsu Science and Technology Association (Grant No. 2020-2-46).

[References]

[1] Li T L. Current situation and prospects of green house industry development in China. Journal of Shenyang Agricultural University, 2005; 36(2): 131–138. (in Chinese)

[2] Yan S J, Wang T S, Zhang Y, Xu S Y, Luo G W. The evolution and development of solar greenhouse technology. Agricultural Science & Technology and Equipment, 2013; 6: 97–98. (in Chinese)

[3] Zhang X B, Song X Q, Zhong Y F, Li C R. Overview of greenhouse development in China. Northern Horticulture, 2001; 2: 1–2. (in Chinese)

[4] Tong G H, Wang T L, Bai Y K, Liu W H. Heat transfer property of wall in solar greenhouse. Transactions of the CSAE, 2003; 19(3): 186–189. (in Chinese)
[5] Zhang L Y, Xu G Y, Ma C W, Lan Y. Application of aerated concrete in salor greenhouse. Journal of Shenyang Agricultural University, 2006; 37(3): 459–462. (in Chinese)
[6] Wang Z, He B, Zou Z R, Wang J W. Thermal environment research on solar greenhouses in plateau and non-cultivated land. Acta Agriculturae Boreali-occidentalis Sinica, 2017; 26(8): 1230–1238. (in Chinese)
[7] Zhao S M, Zhuang Y F, Zheng K X, Ma C W, Cheng J Y, Ma C, et al. Thermal performance experiment on air convection heat storage wall with cavity in Chinese solar greenhouse. Transactions of the CSAE, 2018; 34(4): 223–231. (in Chinese)
[8] Wang H L, Li X Y, Zou Z R. Application of brick wall with phase change rice husk in solar greenhouse. Transactions of the CSAE, 2011; 27(5): 253–257. (in Chinese)
[9] Bai Y K, Liu W H, Wang T L, Li T L. Test and analysis of thermal insulation of aluminum foil embellished polyphenylene panel hollow wall. New Build Mater, 2006; 1: 43–45. (in Chinese)
[10] Li M, Wei X M, Qi F, Zhou C J. Research progress in wall of solar greenhouses. Xinjiang Agriculture Sciences, 2014; 51(6): 1162–1170, 1176. (in Chinese)
[11] Wang X D, Ma C W, Wu L T, Zhang L. Characteristic research and performance optimization of the solar greenhouse wall. Xinjiang Agricultural Sciences, 2009; 46(5): 1016–1021. (in Chinese)
[12] Li Y m, Liu X G, Qi F S, Li W, Li T L. Numerical investigation of the north wall passive thermal performance for Chinese solar greenhouse. Thermal Science, 2020; 24(6): 3465–3476.
[13] Liu Z J, Zheng W G, Hu Q H, Shi Y J, Teng H F. Current situation and development on structure optimization of solar greenhouse in China. Chinese Agricultural Science Bulletin, 2007; 23(2): 449–453. (in Chinese)
[14] Shang Y. Analysis on the current situation and optimization strategy of statistics teaching in China. Insight-Statistics, 2020; 3(1): 19–22.
[15] Qiu C. Empirical study of big data mining technology in English teaching integration and optimization analysis. In: 2020 International Conference on Computers, Information Processing and Advanced Education (CIPAE 2020), Ottawa, Canada: ACM, 2020; pp.495–499. doi: 10.1145/3419635.3419734.
[16] Zhang J, Zou Z R, Zhang Y, Sun Y C. Performance of heating storage gravel wall solar greenhouse. Northern Horticulture, 2016; 2: 46–50. (in Chinese)
[17] Bao E C, Zhu C, Cao Y F, Sun Y C, He B, Mi X, et al. Thermal performance test of solidified sand heat storage wall in Chinese solar greenhouse. Transactions of CSAE, 2017; 33(9): 187–194. (in Chinese)
[18] Li Y M, Yue X, Zhao L, Xu H, Liu X G, Li T L. Effect of north wall internal surface structure on heat storage-release performance and thermal environment of Chinese solar greenhouse. Journal of Building Physics, 2022; 45(4): 507–527.
[19] Arnaoutakis N, Vouros A P, Milousi M, Caouris Y G, Panaras G, Tourlidakis A, et al. Design, energy, environmental and cost analysis of an integrated collector storage solar water heater based on multi-criteria methodology. Energies, 2022; 15(5): 1–21.
[20] Fazelpour F, Bakhshayesh A, Alimohammadi R, Saraei A. An assessment of reducing energy consumption for optimizing building design in various climatic conditions. International Journal of Energy and Environmental Engineering, 2022; 13(1): 319–329.
[21] Yang X L, Wang H L, Xu H J, Han L R. Performance of phase change thermal storage wallboard of disodium hydrogen phosphate dodecahydrate in solar greenhouses. Journal of Shanghai Jiaotong University (Agricultural Science), 2014; 32(4): 88–94. (in Chinese)
[22] Agrafiotis C, Tescari S, Roeb M, Schmücker M, Sattler C. Exploitation of thermochemical cycles based on solid oxide redox systems for thermochemical storage of solar heat. Part 3: Cobalt oxide monolithic porous structures as integrated thermochemical reactors/heat exchangers. Solar Energy, 2015; 114: 459–475.
[23] Yang Y, Li Y J, Yan X Y, Zhao J L, Zhang C X. Development of thermochemical heat storage based on $CaO/CaCO_3$ cycles: A review. Energies, 2021; 14(20) 1–26.
[24] Ding P C, Hou Y B, Han D, Zhang X, Cao S X, Li C Q. Effect of freeze-thaw cycles on mechanical and microstructural properties of tailings reinforced with cement-based material. Minerals, 2022; 12(4): 413. doi: 10.3390/min12040413.
[25] Zou Z, Bao E, Shen T. Design and practice of modular solar greenhouse structure. Appl Eng Tech, 2017; 37: 55–60.
[26] Fan X C, Hu Y C, Meng Y. Experimental research on mechanics performance of modified performance aggregate lightw eight concrete. Concrete, 2017; 11: 94–99. (in Chinese)
[27] Bhat A H, Naqash J A. Experimental studies of sustainable concrete modified with colloidal nanosilica and metakaolin. Journal of Building Pathology and Rehabilitation, 2021; 7: 18. doi: 10.1007/s41024-021-00157-8.
[28] Gadag P R, Somasekharaiah H M, Ghorpade V, Ghorpade V, Rao H S. Evaluation of strength parameters of metakaolin and nanosilica incorporated high-performance concrete. IOP Conference Series: Earth and Environmental Science, 2021; 822: 012029. doi: 10.1088/1755-1315/822/1/012029.
[29] Guo R X, He K C, Ma Q M, Yan F, Lin Z, Sun Y L. Compressive properties and microstructure of modified lightweight aggregate concrete after exposure to elevated temperatures. Journal of Building Materials, 2017; 20(3): 333–338. (in Chinese)
[30] Zhu C, Sun Y C, He B, Bao E C, Zhang Y, Zou Z R. Analysis of performance for back wall of initiative heat storage of solidified sand on solar greenhouse. Northern Horticulture, 2017; 9: 46–52. (in Chinese)
[31] Wang C C, Bao E C, Liu L, Zou Z R, Kang D, Zhou H Y. Performance analysis of solar greenhouse after active lighting and phase change heat storage technological transformation. Northern Horticulture, 2018; 6: 56–61. (in Chinese)
[32] Guo H Q, Li Z H, Zhang Z W, Cui Y A, Wu D R. The relationship between the north wall construction and interior temperature environment in solar greenhouse. Journal of Shengyang Agricultural University, 1995; 26(2): 193–199. (in Chinese)
[33] Rais S I, Mansoor A, Ahmed N, Shah S T H, Sultana B. Relationship between emissions of carbon dioxide from the cement industry, health expenditures and economic growth in Pakistan. iRASD Journal of Economics, 2021; 3(2): 133–142.
[34] Nimish G, Bharath H A, Lalitha A. Exploring temperature indices by deriving relationship between land surface temperature and urban landscape. Remote Sensing Applications: Society and Environment, 2020; 18: 100299. doi: 10.1016/j.rsase.2020.100299.
[35] Xing L. Simulation of the heat environment of tilt-style solar greenhouse in winter. MS dissertation. Harbin: Harbin Institute of Technology, 2006; 92p. (in Chinese)